

## Supplemental information

### Materials

$K_3Fe(CN)_6$ ,  $K_4Fe(CN)_6$ , Acrylamide (AM), Lithium chloride anhydrous (LiCl), N,N'-Methylenebisacrylamide (MBA), and 1-Hydroxycyclohexyl phenyl ketone were purchased from Macklin. Platinum wires with a diameter of 0.3 mm were used as electrodes. Unless otherwise specified, all water used in experiments was deionized water.

### Methods

#### Preparation of LiCl-PAM gel

Firstly, 0.8 g of LiCl, 2.5 g of AM, and 0.03 g of MBA were added sequentially to 10 mL of water, and the mixture was stirred uniformly for 2 minutes. Then, 0.04 g of 1-hydroxycyclohexyl phenyl ketone was incorporated as a photo-initiator, and stirring continued for an additional 10 minutes. After ultrasonic defoaming the obtained solution for 20 minutes, it was immediately transferred to a rectangular mold. At room temperature, the solution was polymerized using UV light with a wavelength of 365 nm for 5 minutes to obtain a LiCl-PAM gel. The mold dimensions were 5 cm × 1.5 cm, with the solution for photopolymerization in each mold being 2 mL. The vertical distance between the light source and the mold was 18 cm.

#### Preparation of SCGPG

The SCGPG was prepared using a two-end soaking method. After adding 1 mL of the soaking solution on the two outer sides of the LiCl-PAM gel, a glass rod was used to quickly scrape and cover an area of 2.2 cm × 1.5 cm on each side, leaving a 0.6 cm × 1.5 cm area in the middle untreated. The gel was allowed to soak for 30 minutes, then assembled with platinum wire electrodes to form the SCGPG, with a 1 cm distance between the electrodes. To prevent water loss during subsequent testing, the samples were encapsulated with polyacrylate tapes (VHB 4905, 3M Company) (Note S1). Vertical cutting was used for tests requiring cutting. The 28 SCGPGs were coupled in series using 0.3 mm platinum wire electrodes to form the 28-SCGPG (Figures 5A and 5B).

### Characterization

The voltage and current data were recorded on an electrochemical workstation (760E, CHI) and a voltmeter (VC869C, Victor). The cyclic voltammetry (CV) measurements were scanned from -0.6 V to +0.6 V on the electrochemical station (760E, CHI). The ionic concentrations were detected by ultraviolet-visible (UV-vis) spectra with a UV-Vis spectrophotometer (UV1900, Shimadzu). Raman spectra were recorded on a Renishaw InVia laser Raman spectrometer using a laser excitation of 514.5 nm (the sampling position and dimensions were the same as those in the UV-vis absorption testing (Figure S7; Note S7), and the cut gel was used directly for Raman spectroscopy testing). Fourier transform infrared (FTIR) spectra were recorded using an FTIR spectrometer (Spectrum One, Perkin Elmer). X-ray photoelectron spectroscopy (XPS) measurements were performed using a Thermo Scientific spectrometer (K-Alpha) with a monochromatic Al K $\alpha$  source. The thermal conductivity ( $\kappa$ ) was calculated via the equation:  $\kappa = c \times \rho \times \alpha$ , in which the specific heat ( $c$ , J g<sup>-1</sup> K<sup>-1</sup>) was measured by differential scanning calorimetry (DSC) at a scanning rate of 5 K min<sup>-1</sup> (DSC 200 F3 Maia, Netzsch), the density of the SCGPG ( $\rho$ , g cm<sup>-3</sup>) was calculated by mass and volume, and the thermal diffusivity ( $\alpha$ , m<sup>2</sup> s<sup>-1</sup>) was measured by the laser-flash diffusivity instrument (LFA 467, Netzsch). The photos and videos were both taken with an iPhone XS Max.

### Note S1. Preventing moisture loss

Since LiCl enhanced the material's water absorption capacity but could not prevent moisture loss at room temperature or under heat, the gel was sealed with 3M polyacrylate tape to maintain stability, with all subsequent tests similarly sealed.<sup>1</sup> Specifically, for the thermal stability of the LiCl-PAM gel, it took about 2 minutes to absorb moisture from the closed environment after heating, followed by corresponding infrared tests (Figure 1B). Electrochemical, heating, and application tests also used 3M tape, while the 28-SCGPG was protected with cling film. As the 3M tape began to deform at temperatures above 70°C, thermal stability assessments were limited to 70°C or lower, with all other tests conducted within this range.

For the water absorption capacity test, the water uptake and swelling ratio of the LiCl-PAM gel were measured after immersion, relative to the sample dried at 70°C for two hours. The water uptake ratio was calculated as:

$$W = \frac{M_w - M_d}{M_d} \times 100\% \quad \text{\* MERGEFORMAT (Equation S1)}$$

Where  $M_w$  referred to the weight of the gel after water absorption, and  $M_d$  denoted the weight of the gel after drying. The swelling ratio was calculated as:

$$S = \frac{V_w - V_d}{V_d} \times 100\% \quad \text{\* MERGEFORMAT (Equation S2)}$$

Where  $V_w$  referred to the volume of the gel after water absorption, and  $V_d$  denoted the volume of the gel after drying.

### Note S2. Performance testing of SCGPG with different soaking modes and concentrations

--SCGPG represented the use of a non-soaked LiCl-PAM gel as the electrolyte. Fi--SCGPG indicated the gel soaked with a 0.4 mol/L  $\text{Fe}(\text{CN})_6^{3-}$  solution on only one side as the electrolyte, while Fo--SCGPG referred to the gel soaked with a 0.4 mol/L  $\text{Fe}(\text{CN})_6^{4-}$  solution on only one side as the electrolyte. Fi+Fo/--SCGPG signified the gel soaked with a mixed solution of 0.4 mol/L  $\text{Fe}(\text{CN})_6^{3-}$  and 0.4 mol/L  $\text{Fe}(\text{CN})_6^{4-}$  on only one side as the electrolyte. Fi+Fo/Fi+Fo-SCGPG referred to the gel soaked with a mixed solution of 0.4 mol/L  $\text{Fe}(\text{CN})_6^{3-}$  and 0.4 mol/L  $\text{Fe}(\text{CN})_6^{4-}$  on both sides as the electrolyte.

The wiring methods for the electrical performance testing of SCGPG subjected to different soaking methods were as follows: For SCGPG with identical soaking on both sides, the positive terminal of the voltmeter was connected to either side; for SCGPG soaked on only one side, the positive terminal of the voltmeter was connected to the soaked side.

Except for the special instructions outlined above, all the mentioned SCGPGs were Fi/Fo-SCGPGs: the gel was soaked with 0.4 M  $\text{Fe}(\text{CN})_6^{3-}$  and 0.4 M  $\text{Fe}(\text{CN})_6^{4-}$ , with the two ion solutions separately dropped onto either side. For all electrical performance testing of SCGPG, the positive terminal of the voltmeter was connected to the side soaked with  $\text{Fe}(\text{CN})_6^{3-}$ . To eliminate the effects caused by the spontaneous dissipation of concentration gradients, SCGPGs began testing after the voltage dropped to the range of 250-255 mV (Note S4), and samples soaked with other concentrations were tested after the same duration following their preparation.

### Note S3. Theoretical analysis of SCGPG

For electrochemical cells, such as thermogalvanic cells, the redox couple ferro/ferricyanide ( $\text{Fe}(\text{CN})_6^{3-}/\text{Fe}(\text{CN})_6^{4-}$ ) undergoes a reversible redox reaction ( $\text{Fe}(\text{CN})_6^{3-} + e^- \leftrightarrow \text{Fe}(\text{CN})_6^{4-}$ ) when a temperature difference is applied between the positive and negative electrodes. According to the Nernst equation, the electrical redox potential ( $E$ ) of this reaction can be expressed as:

$$E = E^0 + \frac{RT}{F} \ln \left( \frac{\alpha_{\text{Fe}(\text{CN})_6^{3-}}}{\alpha_{\text{Fe}(\text{CN})_6^{4-}}} \right) \quad \text{MERGEFORMAT (Equation S3)}$$

Where  $E^0$  is the standard potential,  $\alpha$  is the activity of redox species,  $R$  is the ideal gas constant, and  $F$  is Faraday's constant. The activity ( $\alpha$ ) is defined as the product of the activity coefficient ( $\gamma$ ) and concentration ( $c$ ) ( $\alpha = \gamma \times c$ ). Thus, Eq.(S1) can be expressed as:

$$E = E^0 + \frac{RT}{F} \left[ \ln \left( \frac{\gamma_{\text{Fe}(\text{CN})_6^{3-}}}{\gamma_{\text{Fe}(\text{CN})_6^{4-}}} \right) + \ln \left( \frac{c_{\text{Fe}(\text{CN})_6^{3-}}}{c_{\text{Fe}(\text{CN})_6^{4-}}} \right) \right] \quad \text{MERGEFORMAT (Equation S4)}$$

For SCGPG, the open-circuit voltage ( $V_{oc}$ ) is generated by the difference of  $E$  for the ferricyanide ( $E_{fis}$ ) and the ferrocyanide sides ( $E_{fos}$ ), and thereby can be calculated by:

$$V_{oc} = \frac{RT}{F} \left\{ \left[ \ln \left( \frac{\gamma_{\text{Fe}(\text{CN})_6^{3-}}}{\gamma_{\text{Fe}(\text{CN})_6^{4-}}} \right)_{fis} - \ln \left( \frac{\gamma_{\text{Fe}(\text{CN})_6^{3-}}}{\gamma_{\text{Fe}(\text{CN})_6^{4-}}} \right)_{fos} \right] + \left[ \ln \left( \frac{c_{\text{Fe}(\text{CN})_6^{3-}}}{c_{\text{Fe}(\text{CN})_6^{4-}}} \right)_{fis} - \ln \left( \frac{c_{\text{Fe}(\text{CN})_6^{3-}}}{c_{\text{Fe}(\text{CN})_6^{4-}}} \right)_{fos} \right] \right\} \quad \text{MERGEFORMAT}$$

(Equation S5)

The first term in Eq.(S3) containing the activity coefficient is considered to be dominated by the solvent-dependent difference in entropy between the redox species.<sup>2,3</sup> The large thermopower (nearly a constant  $\sim 1.4 \text{ mV K}^{-1}$ ) in the typical equal-concentration  $\text{Fe}(\text{CN})_6^{3-}/\text{Fe}(\text{CN})_6^{4-}$  system has demonstrated the temperature dependence of  $\gamma$ .<sup>4,5</sup> Therefore, when there is no temperature difference on both sides, the ratio of activity coefficient remains constant, then Eq. (S3) can be simplified to:

$$V_{oc} = \frac{RT}{F} \left\{ \left[ \ln \left( \frac{c_{\text{Fe}(\text{CN})_6^{3-}}}{c_{\text{Fe}(\text{CN})_6^{4-}}} \right)_{fis} + \ln \left( \frac{c_{\text{Fe}(\text{CN})_6^{4-}}}{c_{\text{Fe}(\text{CN})_6^{3-}}} \right)_{fos} \right] \right\} \quad \text{MERGEFORMAT (Equation S6)}$$

The formula shows a positive correlation with both the concentration ratio of  $\text{Fe}(\text{CN})_6^{3-}/\text{Fe}(\text{CN})_6^{4-}$  on the ferricyanide side and the concentration ratio of  $\text{Fe}(\text{CN})_6^{3-}/\text{Fe}(\text{CN})_6^{4-}$  on the ferrocyanide side, indicating the sensitivity of the concentration gradient potential difference to the substance concentration. When the temperature difference between the two sides is zero, the ratio of activity coefficients remains unchanged; however, the concentration of the ion pair is influenced by the migration rate, which varies with the temperature difference. This inspired our work, namely, applying heating to the center of the material while cooling both ends equally, thereby maintaining the ion concentration gradients.

#### Note S4. Output power density and conductivity testing

Typically, the initial voltage of a freshly prepared SCGPG was slightly above 250 mV. To assess its output performance, unless otherwise specified, the initial voltage for all subsequent electrical performance tests was controlled within the range of 250-255 mV. For power density tests, stricter control was applied, with initial voltage fluctuations limited to  $\pm 0.1 \text{ mV}$ . Three types of LSV scans were performed: five SCGPGs with an initial voltage of 252 mV (Figure 4A); a single SCGPG with an initial voltage of 252 mV, where each scan was followed by a 10-minute self-charging (just placed) period before the next scan (Figure 4B); and a single SCGPG with scans starting when the voltage rose to 195 mV after discharge, with each subsequent scan beginning after self-charging to 195 mV (Figure 4C). The scan rates for all three scans were set in the

following order: 100 mV/s, 50 mV/s, 10 mV/s, 5 mV/s, and 1 mV/s.

Due to the spontaneous charging of SCGPG after discharge (Figure 3, Stages 2 and 3), we referred to the discontinuous discharge of SCGPG as the 'charging-included mode', while the tests of Figures 4B and 4C were based on this mode. It should be noted that in Figure 4B, since charging could not reach the initial voltage, the measured current was negative when the open-circuit voltage was lower than the set voltage, resulting in a negative power density. According to Figure 4C, when charging during scan intervals ensured that each scan started from 195 mV, the power density obtained was always greater than zero, which was also observed in Figure 4A.

For the resistance discharge test, the initial voltage of all six samples was 252 mV, and they were discharged under six different resistances. The DM-6210 programmable resistance board was used for the resistances. The current density over a 300-second discharge was recorded, with data recorded every 0.1 seconds. The power was calculated by squaring the current and multiplying it by the resistance, while the power density was obtained by dividing the power by the electrode area. The average value from the last 200 seconds was taken as the actual output power density (Figures 4F and 4G).

For the cyclic discharge performance test, the SCGPG underwent 100 charge-discharge cycles under 3 k $\Omega$ , with an initial voltage of 252 mV. Each discharge and self-charging period lasted 25 seconds.

The conductivity ( $\sigma$ ) was calculated via the equation:  $\sigma = L / (R \times A)$ , where  $L$  and  $A$  represented the electrode spacing and cross-sectional area of the material, respectively.  $R$  was the resistance measured by AC impedance spectroscopy. The conductivity of the SCGPG was measured using electrochemical impedance spectroscopy (EIS).<sup>6</sup> An AC voltage of 0.02 V was applied over a frequency range of 0.1 Hz to 10<sup>5</sup> Hz to construct the Nyquist plot. The Nyquist plot of the SCGPG (Figure 1D) showed that diffusion resistance was the primary contributor to the material's internal resistance. The intercept of the curve with the real axis ( $Z'$ ) indicated that the resistance of the SCGPG was 91  $\Omega$ . The electrode spacing was 1 cm, the material width was 1.5 cm, and the thickness was 0.2 cm. Based on this, the conductivity was calculated to be 3.66 S/m.

Additionally, the conductivity of LiCl-PAM gel was tested at different temperatures (Figure S4). The Nyquist plot of LiCl-PAM gel at different temperatures nearly overlapped, further demonstrating the thermal stability of the gel. However, upon magnifying the high-frequency region of the Nyquist plot, it was observed that when the temperature exceeded 50°C, the regularity of the impedance spectra disappeared. This phenomenon was due to the gel's water loss rate exceeding the water absorption rate in a sealed environment, causing internal resistance to become erratic. To prevent such changes in the gel matrix from affecting the test results, we controlled the temperature applied during the waste heat utilization experiment to below 50°C (Figures S5 and S11). The conductivity of LiCl-PAM gel at different temperature was calculated, showing a slight increase in conductivity with rising temperature. This increase was attributed to the movement of water molecules, but since the evaporation of water in SCGPG was perpendicular to ion migration, this increase may have eventually been reduced further.

#### **Note S5. Charging the commercial capacitor**

For the 28-SCGPG, when the open-circuit voltage decayed to around 4.2 V, the voltage drop tended to stabilize. At this point, charging the capacitor ensured that each capacitor's voltage could reach 4 V, allowing us to compare the duration required for capacitors with varying capacitances to reach the same voltage. The rated voltage of all capacitors was 100 V, and the charging sequence proceeded in the order of 2.2  $\mu$ F, 10  $\mu$ F, 47  $\mu$ F, and 100  $\mu$ F, with an immediate switch to the next capacitor after reaching 4 V.

**Note S6. Temperature measurement of the experiment that used a temperature difference to maintain the concentration gradient.**

For the test controlling temperature (cold at both ends and hot in the middle) to delay concentration dissipation, temperature controllers (TEC207L, Sense Future, with a precision of  $\pm 0.01^\circ\text{C}$ ) were employed on both sides for cooling, while a USB heating pad was used for heating in the middle, with a heating width of 0.5 cm, smaller than the 1 cm distance between the electrodes, ensuring both electrodes maintained the same temperature. The actual temperatures were collected by the TA612C thermometer (TRSi), with an accuracy of  $0.1^\circ\text{C}$ . By adjusting the temperature controller at the cold end, the actual temperature difference between the ends of the SCGPG and the middle was maintained at 10 K (Figure S5), and the concentrations of  $\text{Fe}(\text{CN})_6^{3-}$  and  $\text{Fe}(\text{CN})_6^{4-}$  were measured at the same position after controlling the temperature for different durations. The calculation formula for the temperature difference was:

$$\Delta T = [(T_{hot} - T_{cold1}) + (T_{hot} - T_{cold2})] / 2 \quad \text{MERGEFORMAT (Equation S7)}$$

Where  $T_{hot}$  referred to the heating temperature in the middle,  $T_{cold1}$  represented the temperature on one cold side, and  $T_{cold2}$  denoted the temperature on the other cold side.

**Note S7. Utilizing UV-vis absorption spectroscopy to quantify the concentration**

Different concentrations of  $\text{Fe}(\text{CN})_6^{3-}$  and  $\text{Fe}(\text{CN})_6^{4-}$  standard solutions (0.4 mol/L, 0.3 mol/L, 0.2 mol/L, and 0.1 mol/L) were used to soak the LiCl-PAM gel for 30 minutes. Then, samples of gel measuring  $0.2 \text{ cm} \times 1.5 \text{ cm}$  were immersed in 10 ml of distilled water for 24 hours, which was used for UV-vis absorption testing. The UV-vis absorption spectra were utilized to construct the standard curve (Figure S6).

For the test maintaining the concentration gradient through temperature difference, the duration of the applied temperature difference for different SCGPGs was 10 hours, 20 hours, 30 hours, 40 hours, and 50 hours. Samples measuring  $0.2 \text{ cm} \times 1.5 \text{ cm}$  were cut from positions 0.5 cm to the left and right of the centerline (Figure S7), and then immersed in 10 ml of distilled water for 24 hours, intended for UV-vis absorption testing. The control group consisted of SCGPG samples placed at room temperature for 10 hours, 20 hours, 30 hours, 40 hours, and 50 hours. Based on the Lambert-Beer law of UV-vis absorption spectra,<sup>7</sup> quantitative analysis of the concentrations of  $\text{Fe}(\text{CN})_6^{3-}$  and  $\text{Fe}(\text{CN})_6^{4-}$  was performed.

As shown in Figure S8, it was observed that with the increase in time, the color of the samples on the  $\text{Fe}(\text{CN})_6^{4-}$  side placed at room temperature significantly deepened, while the color change on the  $\text{Fe}(\text{CN})_6^{3-}$  side was not obvious. In contrast, the samples subjected to temperature differences showed a lighter color change on the  $\text{Fe}(\text{CN})_6^{4-}$  side, but the color change on the  $\text{Fe}(\text{CN})_6^{3-}$  side remained subtle, which may have been related to the color change of the solution in its natural state. Figure S9 compared the color changes of 0.4 mol/L  $\text{K}_3[\text{Fe}(\text{CN})_6]$  and 0.4 mol/L  $\text{K}_4[\text{Fe}(\text{CN})_6]$  solutions under natural conditions, revealing that after 2 days, the color of the  $\text{Fe}(\text{CN})_6^{3-}$  solution significantly deepened, while the color change of the  $\text{Fe}(\text{CN})_6^{4-}$  solution was not evident. This explained why the solution color of the  $\text{Fe}(\text{CN})_6^{3-}$  side used for UV spectroscopy testing was deeper and showed little change over time.

**Note S8. Calculation of the concentration gradient retention ratio and the concentration gradient voltage retention ratio**

The concentration gradient retention rate ( $c_r$ ) was calculated as:  $c_r = (c_f / c_i) * 100\%$ , where  $c_f$  was the average concentration gradient of five samples after treatment, and  $c_i$  was the average concentration of five

initial samples. The actual concentration gradient retention rate ( $c_r$ ) was twice the concentration gradient retention rate.

The concentration gradient voltage retention rate ( $V_r$ ) (also called the concentration gradient potential difference retention rate) was calculated as:  $V_r = (V_f / V_i) * 100\%$ , where  $V_f$  was the average voltage of five samples after treatment, while the  $V_i$  was the average voltage of five initial samples.

#### **Note S9. Collecting waste heat from a laptop to maintain the concentration gradient voltage**

In order to demonstrate the role of waste heat in maintaining concentration gradient voltage, we affixed 28 graphite sheets (1.5 cm × 0.5 cm × 0.2 cm, 100 W/(m·K)) to the back of the 28-SCGPG. Each graphite sheet was centrally positioned below the corresponding SCGPG to ensure rapid heat transfer from the bottom to the center of the material, while the heat at both ends was dissipated through the air (about 0.0257 W/(m·K)), thereby establishing a temperature difference with cooler ends and a hotter center. Furthermore, the relatively low thermal conductivity of the material (0.512 W/(m·K)) effectively enhanced the ability to maintain the thermal gradient.

Placed the 28-SCGPG above the laptop (T58, MACHENIKE, the top left area is the main heating zone) and ran the laptop until the surface temperature stabilized. The laptop continuously operated under the same operating mode (CPU usage at 30%, memory usage at 90%, with minor fluctuations), testing the temperatures of six surface positions corresponding to the samples (Figure S10). When the surface temperature reached basic stability (with a fluctuation of 0.3°C), data were recorded every 30 seconds, and the average temperature over 30 minutes was used to determine the temperature at each point (a total of 18 points). The temperature difference at each position was calculated using Equation S5, and the average of the temperature differences from the six areas was taken to obtain the final temperature difference (Figure S11). It was important to note that when there was a temperature difference between the two sides, a certain thermoelectric potential would be generated. However, due to the small temperature difference and the opposite arrangement of our generators, the thermoelectric potentials would cancel each other out, so the influence of this value was neglected. For powering the mouse (M545, Logitech), the test was conducted daily at 9:00 AM, with successful power delivery defined as the indicator light turning on and the mouse being able to slide on the computer (Movie 2).

#### **Note S10. Fabrication and performance testing of water-soil-SCGPG**

Two graphite sheets measuring 3 cm × 0.5 cm × 0.1 cm were inserted vertically into the soil as electrodes, with a distance of 10 cm between them, and connected to the voltmeter to collect voltage data. A mixture of 2 ml detergent (Liby) and 4 ml oil (Golden Dragon Fish) was added to 200 ml of tap water and stirred thoroughly to simulate domestic wastewater. Typically, the soil exhibited a voltage of less than 30 mV, which gradually decreased. To facilitate comparison, soaking was initiated when the voltage changed to 20 mV (Video 3), and it was observed that the voltage increased during soaking at the negative electrode of the wastewater-soil-SCGPG. The soaking methods for rain-soil-SCGPG and lake-soil-SCGPG were also the same, with rainwater collected on July 3, 2024, and February 23, 2025, from Southwest University of Science and Technology, and lake water sourced from the same university.

For the discharge performance test, the initial voltages of wastewater-soil-SCGPG, rain-soil-SCGPG, and lake-soil-SCGPG were 125 mV, 300 mV and 230 mV, respectively. They were discharged under 3 kΩ resistances using the DM-6210 programmable resistance board. The current density was recorded every 0.1 seconds over a 300-second discharge period. Power was calculated by squaring the current and multiplying it

by the resistance, while power density was determined by dividing the power by the electrode area. The average value from the last 200 seconds was taken as the actual output power density (Figure S14).

For the cyclic discharge performance test, the lake-soil-SCGPG underwent 100 charge-discharge cycles under 3 k $\Omega$ , with an initial voltage of 230 mV. Each discharge and self-charging period lasted 25 seconds.

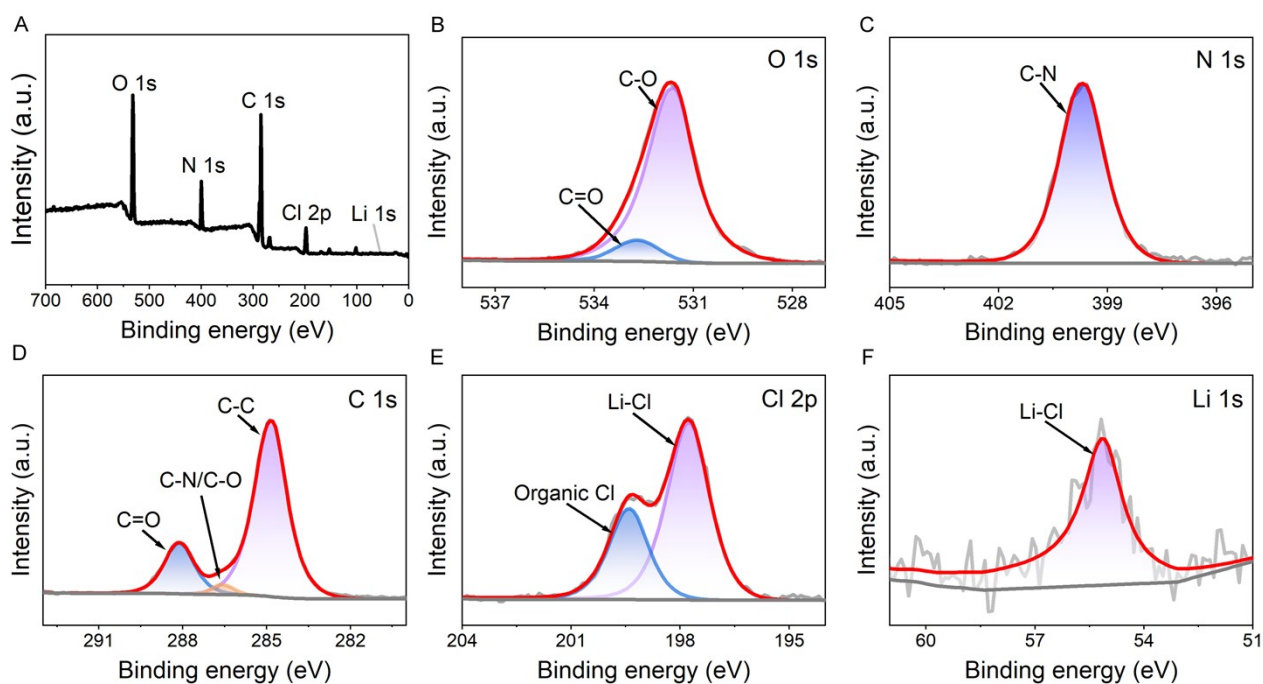


**Figure S1. XPS spectral analysis of the LiCl-PAM gel.** (A) XPS survey spectra of the LiCl-PAM gel. High-resolution XPS spectrum of O 1s (B), N 1s (C), C 1s (D), Cl 2p (E) and Li 1s (F) for LiCl-PAM gel.

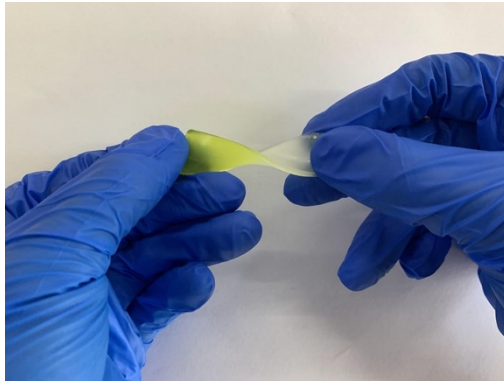


**Figure S2.** Photographs of the twisted SCGPG.

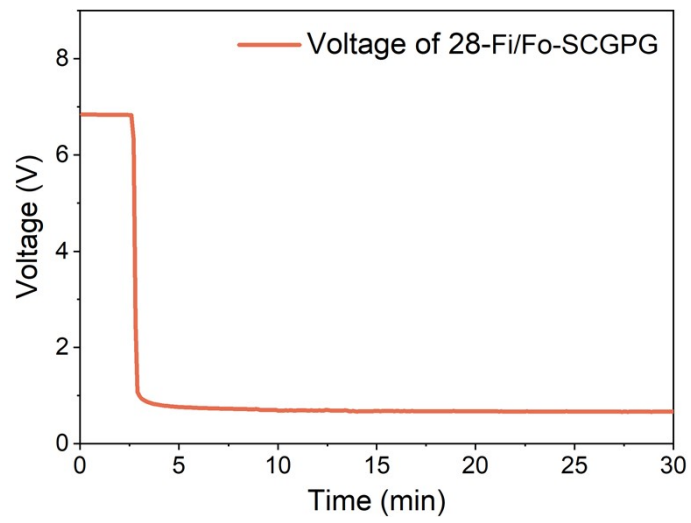


**Figure S3.** The voltage-time curve of 28-SCGPG discharging under a 5 k $\Omega$  resistance. The discharge began at 2.7 minutes.

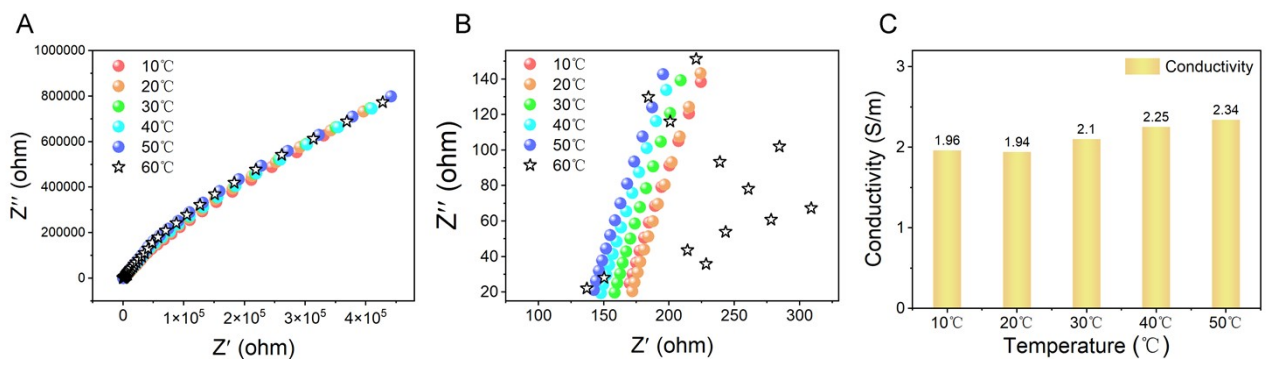


**Figure S4. The conductivity of LiCl-PAM gel at different temperatures.** (A) Nyquist plots of LiCl-PAM gel at different temperatures. (B) Magnified view of the Nyquist plots. (C) Conductivity of LiCl-PAM gel at different temperatures.

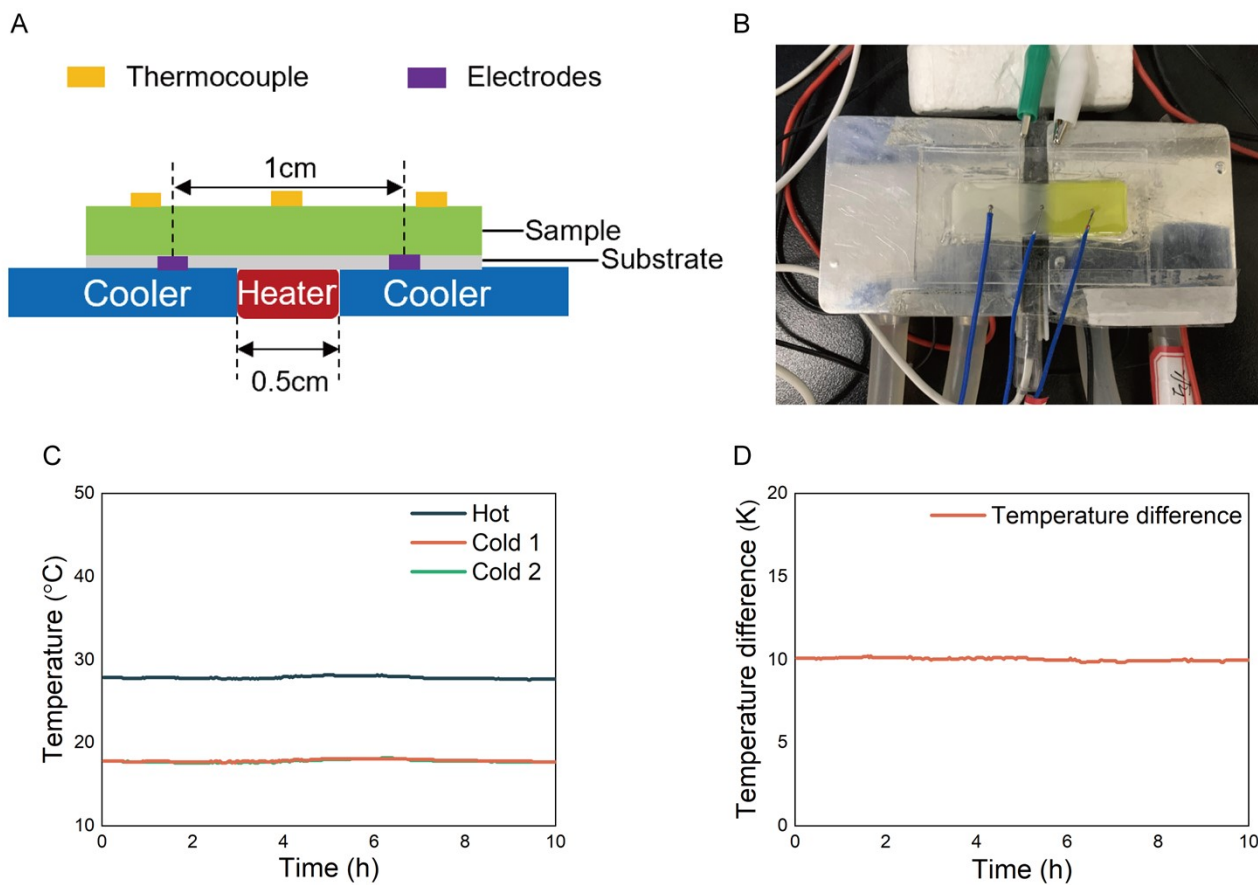


**Figure S5. Temperature measurement of the experiment using temperature difference to maintain concentration gradient.** (A) Schematic diagram of the temperature control device. (B) Photograph of the temperature control device. (C) Plot of the temperature applied to the hot end and the two cold ends of the material. (D) Temperature difference applied to the material.

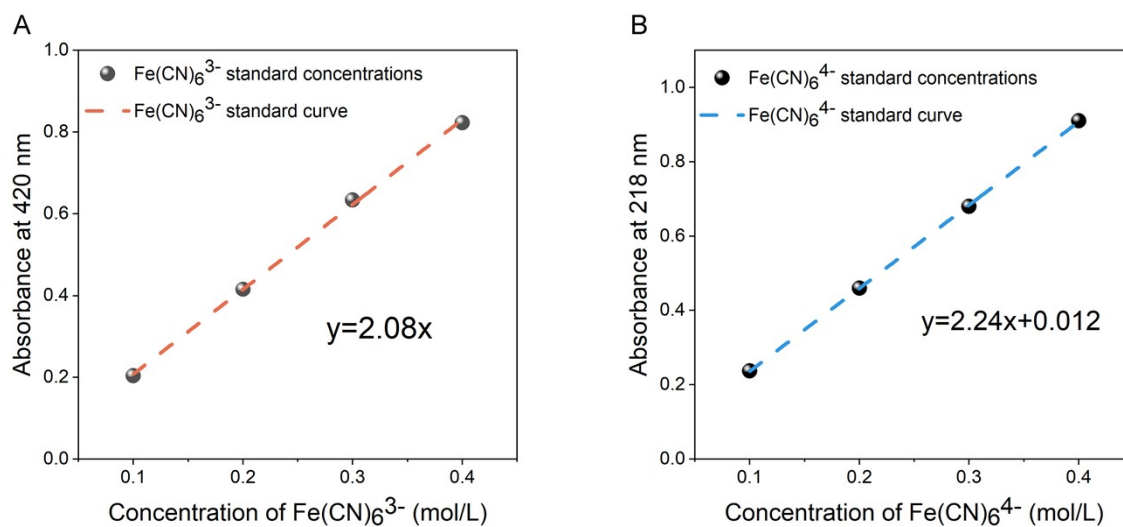


**Figure S6. Standard curve obtained from the immersion liquid of the gel soaked with corresponding standard concentration solution.** (A) Standard curve obtained from the gel soaked with Fe(CN)<sub>6</sub><sup>3-</sup> standard solution. (B) Standard curve obtained from the gel soaked with Fe(CN)<sub>6</sub><sup>4-</sup> standard solution.

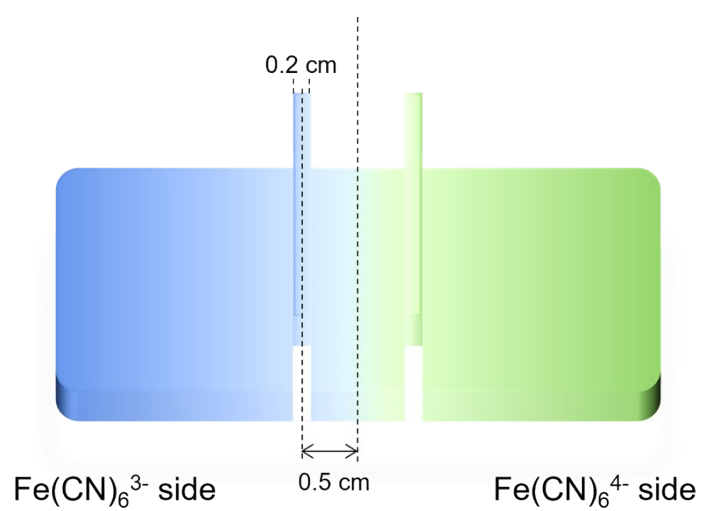
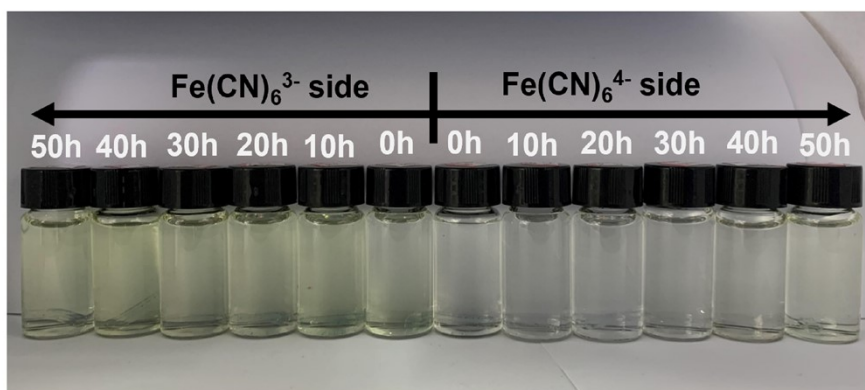


**Figure S7.** Schematic of cutting the sample for UV-vis absorption and Raman spectroscopy testing.

A



B

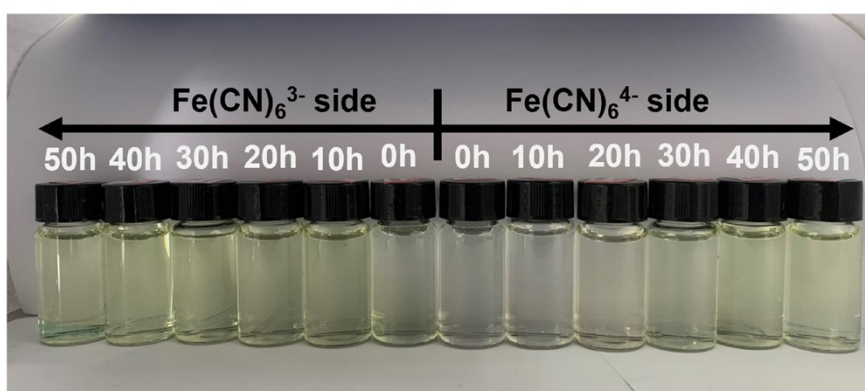


**Figure S8. Photograph of the solution for UV-vis absorption spectra testing after treatment for different durations. (A) Heating treatment. (B) Room temperature treatment.**

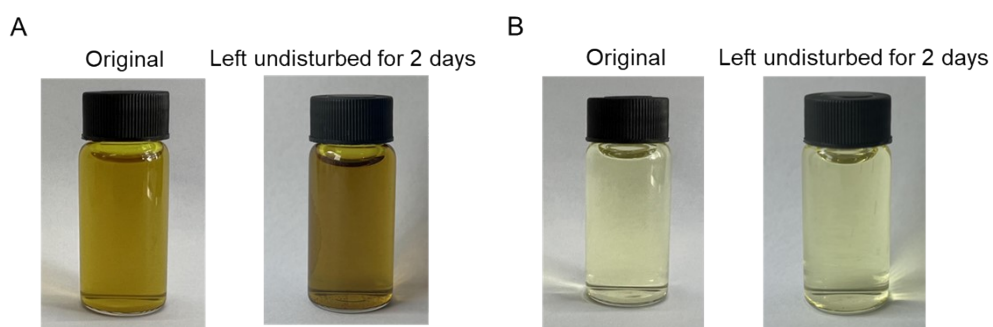


**Figure S9. Color change of the solution after being left undisturbed for 2 days.** (A) 0.4 mol/L  $K_3[Fe(CN)_6]$  solution. (B) 0.4 mol/L  $K_4[Fe(CN)_6]$  solution.

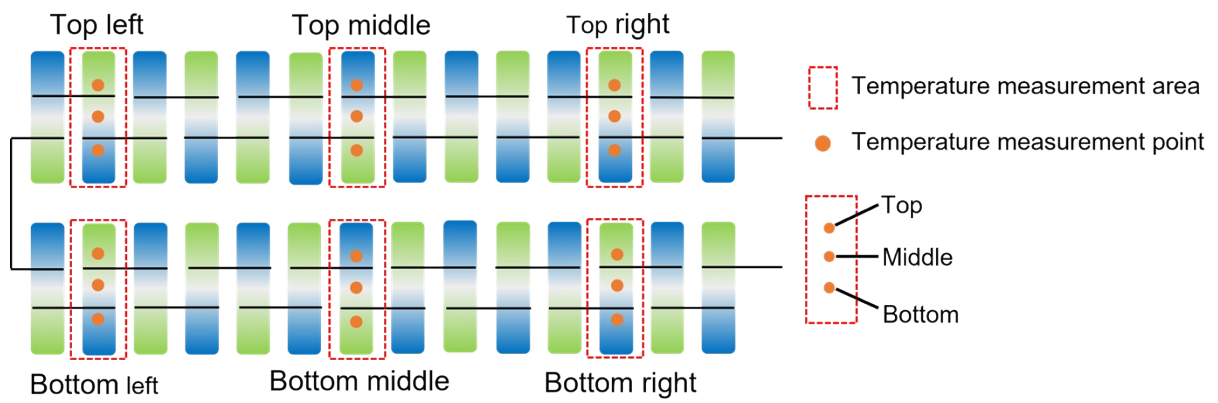


**Figure S10.** Schematic diagram of the temperature measurement locations for heat collection from the laptop.

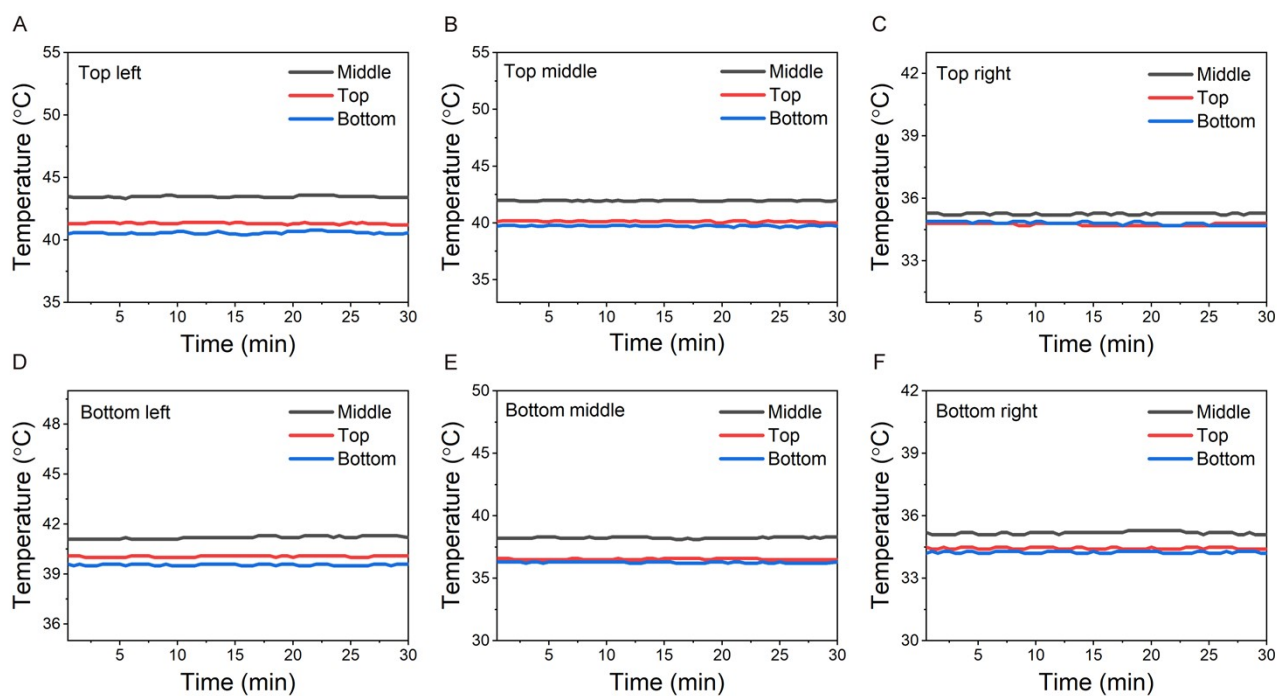


**Figure S11.** Temperature data of the six areas in Figure S10. The average of the temperature differences from the six areas was calculated to be 1.82 K.

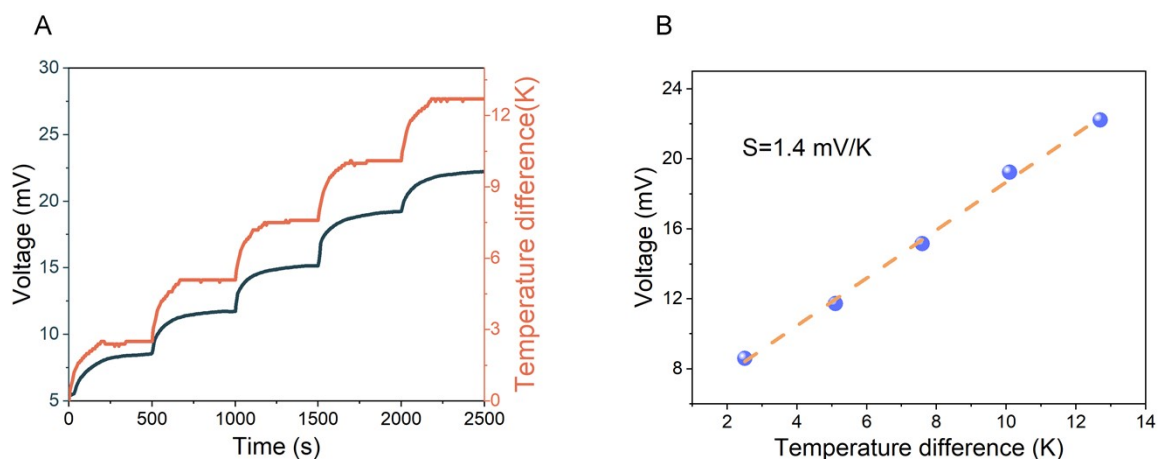


**Figure S12.** Seebeck coefficient of SCGPG after naturally being left for 90 days. The Seebeck coefficient is an important parameter for measuring the thermoelectric performance of materials.<sup>8,9</sup> It is calculated by taking the absolute value of the ratio of the voltage difference to the applied temperature difference. During the measurement, a temperature difference was applied using the method of having one side cold and the other hot, while the corresponding voltage values were recorded. When the voltage values reached basic stability, the temperature was increased for the next measurement.

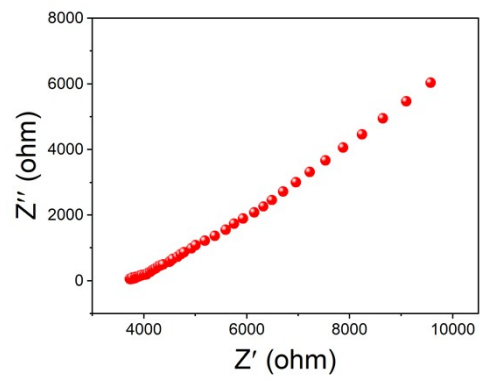


**Figure S13.** The Nyquist plots of soil.

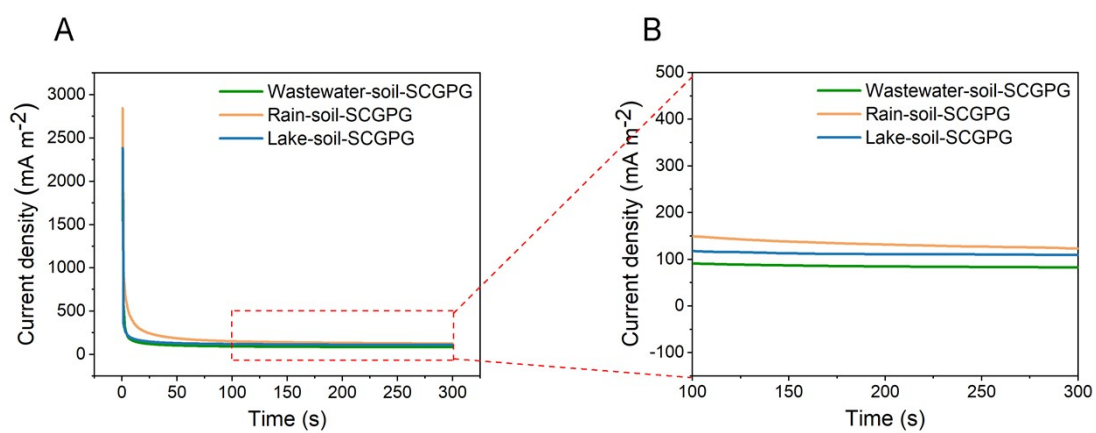


**Figure S14. Current density-time curves of three types of water-soil-SCGPG.** (A) Current density-time curves of three types of water-soil-SCGPG during discharge under 3 k $\Omega$  resistance. (B) Enlarged view of the current density-time curves during the last 200 seconds of discharge under resistance.

**Table S1.** Water absorption capacity of LiCl-PAM gel.

Sample status	Mass (g)	Length (cm)
Initial	1.827	4.8
After drying at 70°C	1.529	4.1
After immersing	1.970	5.2

Movie 1: Demonstration of the power supply application for the calculator and the wiring display of the entire circuit.

Movie 2: Demonstration of utilizing waste heat from the laptop to maintain the concentration gradient and power the mouse.

Movie 3: Preparation of wastewater-soil-SCGPG and the voltage changes during this process.

## Supplemental References

1. Lei, Z., Gao, W., and Wu, P. (2021). Double-network thermocells with extraordinary toughness and boosted power density for continuous heat harvesting. *Joule* 5, 2211–2222. <https://doi.org/10.1016/j.joule.2021.06.003>.
2. Yu, B., Duan, J., Cong, H., Xie, W., Liu, R., Zhuang, X., Wang, H., Qi, B., Xu, M., Wang, Z.L., et al. (2020). Thermosensitive crystallization–boosted liquid thermocells for low-grade heat harvesting. *Science* 370, 342–346. <https://doi.org/10.1126/science.abd6749>.
3. Yu, B., Yang, W., Li, J., Xie, W., Jin, H., Liu, R., Wang, H., Zhuang, X., Qi, B., Liu, S., et al. (2021). Heat-triggered high-performance thermocells enable a self-powered forest fire alarm. *J. Mater. Chem. A* 9, 26119–26126. <https://doi.org/10.1039/D1TA06793A>.
4. Kim, T., Lee, J.S., Lee, G., Yoon, H., Yoon, J., Kang, T.J., and Kim, Y.H. (2017). High thermopower of ferri/ferrocyanide redox couple in organic-water solutions. *Nano Energy* 31, 160–167. <https://doi.org/10.1016/j.nanoen.2016.11.014>.
5. A. Buckingham, M., Laws, K., Cross, E., J. Surman, A., and Aldous, L. (2021). Developing iron-based anionic redox couples for thermogalvanic cells: towards the replacement of the ferricyanide/ferrocyanide redox couple. *Green Chemistry* 23, 8901–8915. <https://doi.org/10.1039/D1GC02989D>.
6. Akbar, Z.A., Malik, Y.T., Kim, D.-H., Cho, S., Jang, S.-Y., and Jeon, J.-W. (2022). Self-Healable and Stretchable Ionic-Liquid-Based Thermoelectric Composites with High Ionic Seebeck Coefficient. *Small* 18, 2106937. <https://doi.org/10.1002/sml.202106937>.
7. Zhao, Y., Ding, C., Zhu, J., Qin, W., Tao, X., Fan, F., Li, R., and Li, C. (2020). A Hydrogen Farm Strategy for Scalable Solar Hydrogen Production with Particulate Photocatalysts. *Angew Chem Int Ed Engl* 59, 9653–9658. <https://doi.org/10.1002/anie.202001438>.
8. Le, Q., Chen, Z., Cheng, H., and Ouyang, J. (2023). Giant Thermoelectric Performance of N-Type Ionogels by Synergistic Dopings of Cations and Anions. *Advanced Energy Materials* 13, 2302472. <https://doi.org/10.1002/aenm.202302472>.
9. Li, X., Zhang, G., Zhang, X., Zou, W., Li, G., Zhang, X., Li, Y., Zhang, L., Wang, M., Chen, B., et al. (2023). Transparent charge transfer complex with high thermoelectric performance. *Joule* 7, 2814–2829. <https://doi.org/10.1016/j.joule.2023.10.008>.